

Adsorption rate of Reactive Black 5 on chitosan based materials: geometry and swelling effects

G. L. Dotto¹ · R. Ocampo-Pérez² · J. M. Moura³ · T. R. S. Cadaval Jr.³ · L. A. A. Pinto³

Received: 9 April 2016/Revised: 2 August 2016/Accepted: 5 August 2016/Published online: 11 August 2016
© Springer Science+Business Media New York 2016

Abstract The overall adsorption rate of Reactive Black 5 dye (RB5) on chitosan based materials was elucidated using diffusional models. Fundamental aspects, such as, geometry of the adsorbents and swelling effects were considered. Chitosan based materials (powder and film) were prepared from shrimp wastes and characterized regarding to the fundamental features for adsorption. Experimental decay curves were obtained under different conditions of stirring rate and initial dye concentration. The data were modeled according to the external mass transfer and diffusional models. The k_L (external mass transfer coefficient), D_{ep} (effective pore diffusion coefficient) and D_s (surface diffusion coefficient) values were estimated.

For both adsorbents, it was found that the surface diffusion was the intraparticle diffusion mechanism governing the adsorption rate of RB5, since its contribution was higher than 92 % regardless the position and time. The D_s values ranged from 2.85×10^{-11} to 5.78×10^{-11} for chitosan powder and from 4.15×10^{-11} to 12.12×10^{-11} $\text{cm}^2 \text{s}^{-1}$ for chitosan films. The RB5 adsorption was faster when chitosan powder was used, mainly at higher stirring rates and initial dye concentrations. The swelling effect was most pronounced for the chitosan films, where, provided an increase of about 65 times in the D_s value.

Keywords Chitosan films · Chitosan powder · Reactive Black 5 · Mass transfer · Swelling

✉ G. L. Dotto
guilherme_dotto@yahoo.com.br

R. Ocampo-Pérez
raul.ocampo@uaslp.mx

J. M. Moura
jaquefurg@gmail.com

T. R. S. Cadaval Jr.
titoeq@gmail.com

L. A. A. Pinto
dqmpinto@furg.br

¹ Environmental Processes Laboratory, Chemical Engineering Department, Federal University of Santa Maria – UFSM, 1000 Roraima Avenue, Santa Maria, RS 97105-900, Brazil

² Facultad de Ciencias Químicas, Centro de Investigación y Estudios de Posgrado, Universidad Autónoma de San Luis Potosí, Av. Dr. M. Nava, 6, San Luis Potosí, SLP 78210, Mexico

³ Industrial Technology Laboratory, School of Chemistry and Food, Federal University of Rio Grande-FURG, 475 Engenheiro Alfredo Huch street, Rio Grande, RS 96203-900, Brazil

List of symbols

ARE	Average relative error (%)
C_A	Dye concentration in bulk solution (mg L^{-1})
C_{Ar}	Dye concentration within the adsorbent varying with position and t (mg L^{-1})
C_{A0}	Initial dye concentration in bulk solution (mg L^{-1})
C_{Ae}	Dye concentration in bulk solution at equilibrium (mg L^{-1})
$C_{A,exp}$	Experimental value of C_A (mg L^{-1})
$C_{A,pred}$	Predicted value of C_A (mg L^{-1})
D_{AB}	Molecular diffusion coefficient ($\text{cm}^2 \text{s}^{-1}$)
D_{ep}	Effective pore volume diffusion coefficient ($\text{cm}^2 \text{s}^{-1}$)
D_s	Surface diffusion coefficient ($\text{cm}^2 \text{s}^{-1}$)
k_L	External mass transfer coefficient ($\text{cm}^2 \text{s}^{-1}$)
K_L	Langmuir constant (L mg^{-1})
m	Mass of adsorbent (g)
M_B	Molecular weight of water (g mol^{-1})

N_{AP}	Mass flux due pore volume diffusion ($\text{mg L}^{-1} \text{cm s}^{-1}$)
N_{AS}	Mass flux due surface diffusion ($\text{mg L}^{-1} \text{cm s}^{-1}$)
q_t	Mass of dye adsorbed per gram of adsorbent (mg g^{-1})
q	Mass of dye adsorbed varying with position and t (mg g^{-1})
q_e	Mass of dye adsorbed at equilibrium (mg g^{-1})
q_m	Maximum adsorption capacity from Langmuir model (mg g^{-1})
r	Radial coordinate varying from 0 to R , R_p (cm)
R^2	Coefficient of determination, dimensionless
S	External surface area per mass of adsorbent ($\text{cm}^2 \text{g}^{-1}$)
t	Time (min or s)
V	Volume of solution (L or m^3)
V_A	Molar volume of solute at its normal boiling temperature ($\text{cm}^3 \text{mol}^{-1}$)
x	Cartesian coordinate, cm

Greek symbols

α	r^2 (spherical coordinates) or 1 (Cartesian coordinates)
ε_p	Void fraction, dimensionless
η_B	Viscosity of water (cp)
ρ_p	Apparent density of the adsorbent (g L^{-1})
ρ_s	Solid density of the adsorbent (g L^{-1})
ξ	r (spherical coordinates) or x (Cartesian coordinates)
ϕ	Association parameter of water, dimensionless
ϕ_A	C_A/C_{A0} , dimensionless

1 Introduction

Reactive dyes, such as Reactive Black 5 (RB5), are commonly used in several industries as textile, leather and paper (Erdem et al. 2016). A certain amount of dyes is wasted during the process and released into the industrial waters, generating colored effluents (Koprivanac and Kusic 2008). It is estimated that the concentration of reactive dyes remained in effluents is around 1000 mg L^{-1} (Su et al. 2016). The incorrect disposal of colored effluents causes severe environmental impacts, and so, these should be carefully treated before discharge (Srinivasan and Viraraghavan 2010). Some operations, including, photocatalytic oxidation (Mehrojoui et al. 2015), bacterial decolorization (Saratale et al. 2011), coagulation/flocculation (Verma et al. 2012), biosorption (Dotto et al. 2015), adsorption (Franco et al. 2015) and other technologies are commonly used to treat dye containing effluents. Among these, adsorption is considered one of the most effective processes of wastewater treatment, due advantages, such as, low cost, ease of operation and high efficiency (Yagub et al. 2014). There are various adsorbent materials used to remove dyes from aqueous solutions, including, agricultural wastes (Salleh et al.

2011), peels (Gupta and Suhas 2009), activated carbons (Demirbas 2009), chitosan based materials (Vakili et al. 2014) and others (Ali et al. 2012).

Chitosan is a polycationic biopolymer, which can be obtained from renewable sources and has unique characteristics, such as, high reactivity, chemical stability and high affinity towards dyes, since contains amino and hydroxyl groups in its structure, promoting adsorbate–adsorbent electrostatic interactions (Crini and Badot 2008). Therefore, chitosan based materials (powder, films, membranes, sponges or fibers), with different geometries and swelling properties, are largely employed to remove dyes from aqueous media (Crini and Badot 2008; Rêgo et al. 2013; Dotto et al. 2014; Esquerdo et al. 2014). Kyzas et al. (2010) studied the adsorption behavior of two dyes on several chitosan derivatives. According to these authors, the diffusion mechanisms were compatible with the expected adsorbent–dye interactions based on their chemical structure. In a previous work (Dotto and Pinto 2011), the removal of acid blue 9 and food yellow 3 onto chitosan was investigated by analyzing the effect of the stirring rate on the adsorption capacity and adsorption rate. The kinetic behavior was analyzed through the pseudo-first order, pseudo-second order, Elovich and Weber–Morris models. The results evidenced that the stirring rate considerably affect the adsorption rate at the initial stages. The pseudo-second order and Elovich models satisfactory interpreted the decay concentration curves and, by the application of Weber–Morris model it was found that intraparticle diffusion and external mass transfer play a main role in the overall adsorption rate of dyes on chitosan. He et al. (2016) synthesized a hybrid membrane (chitosan/oxidized starch/silica) for the removal of two direct dyes (Blue 71 and Red 31). The kinetic data were fitted with kinetic models (pseudo-first order, pseudo-second order) and the results evidenced that pseudo-second order kinetic model best interpreted the experimental data.

The reaction models (pseudo-first order and pseudo-second order) assume that the adsorption kinetics is exclusively controlled by the adsorption rate of the solute on the surface of the adsorbent, and it can be represented as a chemical reaction (Qiu et al. 2009). In some cases, these models are adequate to predict the adsorption rate, but from these models, it is not possible to infer physical interpretations based on the mass transfer mechanisms (Dotto and Pinto 2011; Dotto et al. 2014). On the other hand, the diffusional models take into account the external mass transfer, intraparticle diffusion (pore volume diffusion, surface diffusion, or a combination of both mechanisms) and adsorption on an active site (Ruthven 1984; Suzuki 1990; Ocampo-Pérez et al. 2010, 2011, 2012). Therefore, employing diffusional models, the overall adsorption rate can be represented more realistically.

This work aimed to elucidate in detail the overall adsorption rate of RB5 dye onto chitosan based materials,

taking into account the geometry and swelling effects. For this purpose, several adsorption decay curves were constructed under different experimental conditions, using chitosan powder and chitosan film as adsorbents. These curves were modeled according to the external mass transfer and diffusional models.

2 Mathematical models

2.1 External mass transfer model (EMTM)

This model was developed assuming that the external mass transport controls the overall adsorption rate. In other words, the intraparticle diffusion is instantaneous, so, there is not a concentration gradient inside the particle. Therefore, the intraparticle diffusion resistance is considered to be insignificant. The EMTM model can be expressed mathematically by the Eqs. (1–4):

$$V \frac{dC_A}{dt} = -mSk_L(C_A - C_{Ar}|_{r=R}) \tag{1}$$

$$t = 0 \quad C_A = C_{A0} \tag{2}$$

$$\frac{m\varepsilon_p}{\rho_p} \frac{dC_{Ar}|_{r=R}}{dt} + m \frac{dq_t}{dt} = mSk_L(C_A - C_{Ar}|_{r=R}) \tag{3}$$

$$t = 0 \quad C_{Ar} = 0, q = 0 \tag{4}$$

2.2 Diffusional models

The diffusional models deduced in this study were based on the following assumptions: (i) intraparticle diffusion occurs by pore volume diffusion (Fick diffusion) and surface diffusion; (ii) the adsorption rate on an active site is instantaneous; and (iii) chitosan particles have spherical or film form. The general diffusional model is represented by the Eqs. (5–10) (Ruthven 1984; Suzuki 1990; Ocampo-Pérez et al. 2010, 2011):

$$V \frac{dC_A}{dt} = -mSk_L(C_A - C_{Ar}|_{r=R_p}) \tag{5}$$

$$t = 0 \quad C_A = C_{A0} \tag{6}$$

$$\varepsilon_p \frac{\partial C_{Ar}}{\partial t} + \rho_p \frac{\partial q}{\partial t} = \frac{1}{\alpha} \frac{\partial}{\partial \xi} \left[\alpha \left(D_{ep} \frac{\partial C_{Ar}}{\partial \xi} + D_s \rho_p \frac{\partial q}{\partial \xi} \right) \right] \tag{7}$$

$$C_{Ar} = 0 \quad t = 0 \quad 0 \leq r \leq R_p \tag{8}$$

$$\frac{\partial C_{Ar}}{\partial r} \Big|_{r=0} = 0 \tag{9}$$

$$D_{ep} \frac{\partial C_{Ar}}{\partial \xi} \Big|_{r=R} + D_s \rho_p \frac{\partial q}{\partial \xi} = k_L(C_A - C_{Ar}|_{r=R_p}) \tag{10}$$

The model represented by Eqs. (5–10) is the pore volume and surface diffusional model (PVSDM). The parameters k_L , D_s , and D_{ep} correspond to external transport, surface diffusion, and pore volume diffusion mechanisms, respectively. The parameters α and ξ correspond to r^2 and r for spherical coordinates and l and x for cartesian coordinates. The PVSDM model can be simplified by considering that the sole intraparticle diffusion mechanism may be either pore volume diffusion (PVDM) ($D_{ep} \neq 0$, $D_s = 0$) or surface diffusion (SDM) ($D_{ep} = 0$, $D_s \neq 0$). Furthermore, the PVSDM model can be reduced to EMTM model if D_{ep} and D_s are extremely high.

If the adsorption rate on an active site is considered instantaneous, there is a local equilibrium between the dye concentration in the solution within the pore of the material and the mass of dye adsorbed on the surface of the pore. This equilibrium is represented by the adsorption isotherm, which is the mathematical relationship between C_{Ar} and q , being represented by Eq. (11) (Ocampo-Pérez et al. 2012, 2015):

$$q = f(C_{Ar}) \tag{11}$$

3 Experimental

3.1 Reactive Black 5 dye

The anionic textile dye, Reactive Black 5 (RB5) (color index 20505, molar weight of 991.8 g mol^{-1} , $\lambda_{max} = 596 \text{ nm}$, purity of 95 %) was supplied by Sigma-Aldrich (Brazil) and used without further purification. This dye was selected once its presence is common in textile effluents (Chong et al. 2015). The optimized three-dimensional structural formula of RB5 was obtained from MarvinSketch software, version 14.9.22.0, and is presented in Fig. 1. All other reagents utilized were of analytical grade and deionized water was used to prepare all solutions. The RB5 concentration in water was determined by spectrophotometry UV–Vis (Biospectro, SP–22, Brazil) at 596 nm.

3.2 Preparation and characterization of chitosan based materials

Two chitosan based materials with different geometries, i.e. chitosan powder and chitosan film were prepared and used as adsorbents. Chitosan powder (CPW) was obtained from shrimp wastes (*P. brasiliensis*) by the following consecutive steps: demineralization, deproteinization, deodorization, deacetylation, purification and spouted bed drying. After these steps, CPW with mean diameter of

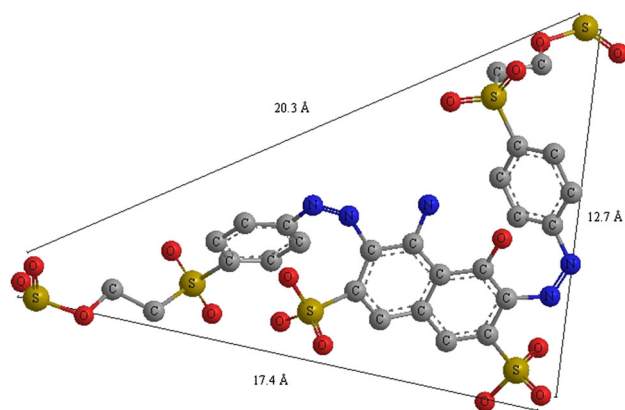


Fig. 1 Optimized chemical structure of the Reactive Black 5 (RB5) dye

$72 \pm 3 \mu\text{m}$, deacetylation degree of $95 \pm 1 \%$ and molecular weight of $150 \pm 3 \text{ kDa}$ was obtained (Dotto et al. 2011; Moura et al. 2015).

Chitosan films (CFS) were obtained from chitosan powder as follows: CPW was dissolved in acetic acid solution by moderate stirring (Marte, MAG–01H, Brazil) at room temperature. The solution was centrifuged (Fanem, 206 BL, Brazil) and was poured onto a level Plexiglas plates. CFS were obtained by solvent evaporation and conditioned in desiccators prior to the use. After this procedure, CFS with thickness of $62 \pm 2 \mu\text{m}$, tensile strength of $39.2 \pm 0.1 \text{ MPa}$ and elongation of $15.7 \pm 0.1 \%$ were obtained. For the adsorption assays, CFS were divided in portions of $1 \times 1 \text{ cm}$ (Dotto et al. 2013; Moura et al. 2015).

CPW and CFS were characterized by scanning electron microscopy (SEM) Jeol, JSM–6610LV, Japan (Goldstein et al. 1992) and Fourier transform infrared spectroscopy (FTIR) (Prestige, 21210045, Japan) (Silverstein et al. 2007). Textural characteristics of the materials (external surface area (S), void fraction (ε_p), solid density (ρ_s), particle density (ρ_p) and swelling properties) were obtained by N_2 -adsorption, helium pycnometry and swelling assays (Brunauer et al. 1938; Dotto et al. 2013; Moura et al. 2015).

3.3 Adsorption isotherms

Batch adsorption experiments were performed in a jar-test (Nova etica, 218 MBD, Brazil) at room temperature ($298 \pm 1 \text{ K}$). RB5 stock solutions (2.0 g L^{-1}) were prepared and its pH was adjusted to 4.0 (preliminary tests showed that this pH was the more adequate for RB5 adsorption on CPW and CFS) with buffer disodium phosphate/citric acid solution 0.1 mol L^{-1} (preliminary tests showed that there is not significant interaction between buffer and RB5).

In order to obtain the equilibrium curves, a ratio of 500 mg L^{-1} of the adsorbents (CPW or CFS) were put in contact with RB5 solutions (initial concentration ranging from 50 to 500 mg L^{-1}) and the flasks were stirred at 100 rpm until the equilibrium. The equilibrium was considered when three consecutive measurements of dye concentration remained constant. The amount of RB5 adsorbed per gram of adsorbent at equilibrium ($q_e, \text{ mg g}^{-1}$) was calculated by the Eq. (12):

$$q_e = \frac{(C_{A0} - C_{Ae}) V}{m} \quad (12)$$

3.4 Concentration decay curves

To obtain the concentration decay curves under different stirring rates, a ratio of 500 mg L^{-1} of the adsorbents (CPW or CFS) were put in contact with RB5 solutions at pH 4 and an initial concentration of 100 mg L^{-1} , and the flasks were stirred at 50, 100, 200 and 300 rpm. The variation of the solution pH was negligible. The concentration decay curves at different initial concentrations of RB5 were obtained by using an adsorbent dosage of 500 mg L^{-1} and concentrations of 100, 200 and 300 mg L^{-1} at 300 rpm. Finally, to verify the swelling effect, the adsorbents were pre-swelled for 30 min, with buffer disodium phosphate/citric acid solution. Then, the concentration decay curves were constructed using an adsorbent dosage of 500 mg L^{-1} , stirring rate of 300 rpm and initial RB5 concentration of 100 mg L^{-1} . For all experiments, samples were removed from the solution at different time intervals.

4 Results and discussion

4.1 Characteristics of chitosan based materials

The SEM images of CPW and CFS adsorbents are presented in Fig. 2. This figure shows the great textural differences between the two physical forms of chitosan (CPW and CFS). This justifies the verification of geometry effect on the adsorption rate of RB5. Chitosan powder presented a rigid surface without visible pores and cavities, hindering the transference of colored liquid within the internal structure of the particle. In parallel, chitosan films presented cavities allowing the dye transference inside the porous structure. The FTIR bands and their respective assignments are shown in Table 1. The bands presented in Table 1 are typical of chitosan based materials and confirms the presence of NH_2 and OH groups, which are the main active sites for dyes adsorption (Crini and Badot 2008). The other characteristics are presented in Table 2. It should be highlighted in Table 2 that CPW swelled 11.1 %

Fig. 2 SEM images of **a** chitosan powder ($\times 500$), **b** chitosan powder ($\times 3000$), **c** chitosan films ($\times 500$) and **d** chitosan films ($\times 3000$)

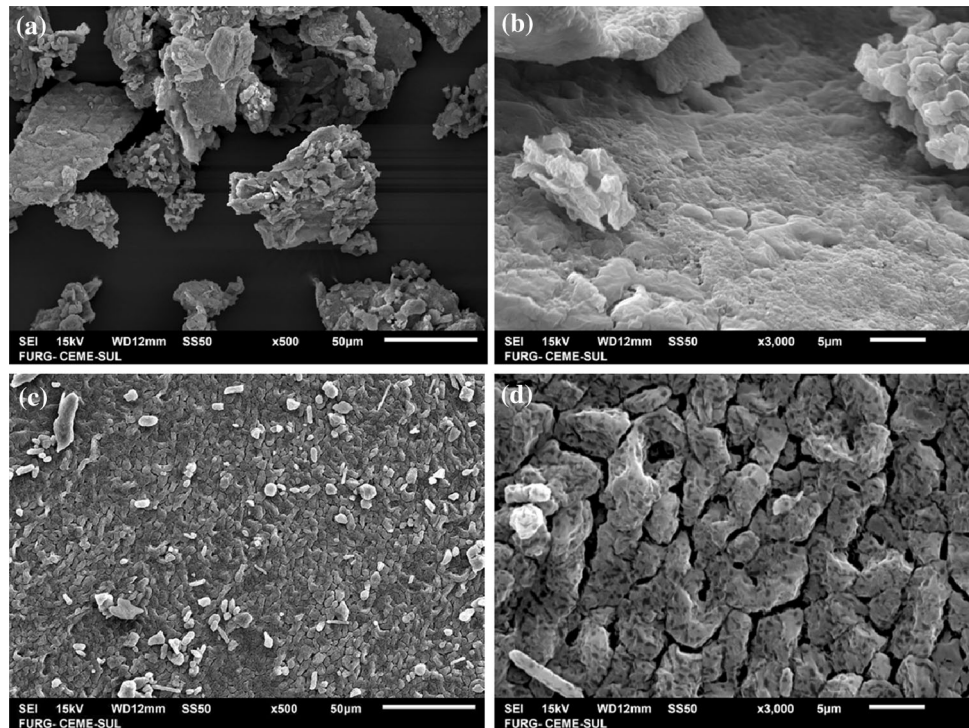


Table 1 FTIR bands of chitosan powder and chitosan films with their respective assignments

FTIR band (wavenumber) (cm^{-1}) ^a	Assignment
3350	N–H stretching
3150	O–H stretching
1550	C–N stretching of amides
1450	Angular deformations of C–O–H and H–C–H
1075	C–N stretching related to the amino groups
680	N–H bending

^a The wavenumbers of CPW and CFS were very similar, since the materials are chemically similar

while CFS swelled 86.2 % (see initial and final dimensions). This information justifies the importance to study the swelling effect on the adsorption rate of RB5.

4.2 Equilibrium curves

The adsorption isotherms are fundamental to establish the mathematical relation between the dye concentration in the

solution within the pore of the adsorbent and the mass of dye adsorbed on the pore surface. This relation is inserted in Eq. (11) and the diffusional model can be solved. The experimental equilibrium curves for the adsorption of RB5 onto CPW and CFS are presented in Fig. 3. In this figure it can be observed that at low equilibrium concentrations the isotherms presented an inclined portion followed by a plateau at high concentrations. Both isotherms showed the

Table 2 Characteristics of chitosan powder and chitosan films

Characteristic	Chitosan powder	Chitosan film
Geometry	Spherical	Cartesian
Initial dimensions ^a	Diameter = $72 \pm 3 \mu\text{m}$	Thickness = $62 \pm 2 \mu\text{m}$
Final dimensions ^a	Diameter = $80 \pm 2 \mu\text{m}$	Thickness = $450 \pm 5 \mu\text{m}$
Void fraction (ϵ_p) ^a	0.05 ± 0.01	0.140 ± 0.02
Solid density (ρ_s) (g L^{-1}) ^a	1550 ± 5	1550 ± 5
Particle density (ρ_p) (g L^{-1}) ^a	1472.5 ± 5	1333.0 ± 5
External surface area (S) ($\text{cm}^2 \text{g}^{-1}$) ^a	566 ± 3	200 ± 2

^a Mean \pm SD (n = 3)

type I behaviour according to the IUPAC classification (Thommes et al. 2015), confirming a high affinity between the adsorbate molecules and adsorbent surface. The experimental data were fitted by using the Langmuir adsorption isotherm model represented by Eq. (13) (Langmuir 1918):

$$q_e = \frac{q_m K_L C_{Ae}}{1 + K_L C_{Ae}} \tag{13}$$

The q_m and K_L values for the RB5 adsorption on chitosan powder and chitosan films are listed in Table 3. The high values of the coefficient of determination ($R^2 > 0.98$) and the low values of average relative error ($ARE < 2.0\%$) show that, in this concentration range, the Langmuir model is adequate to represent the equilibrium adsorption of RB5 on the chitosan based materials (CPW and CFS).

4.3 Concentration decay curves and mass transfer parameters

The external mass transfer coefficient, k_L , was obtained by the correlation proposed by Furusawa and Smith (1973), which was derivate from Eq. (1) by substituting the conditions $t \rightarrow 0$, $C_{Ar} \rightarrow 0$, and $C_A \rightarrow C_{A0}$, and it is represented by Eq. (14):

$$\left[\frac{d\left(\frac{C_A}{C_{A0}}\right)}{dt} \right]_{t=0} = \frac{-mSk_L}{V} \tag{14}$$

The slope of Eq. (14) was evaluated by using the first two points of the concentration decay curve, i.e., for $t = 0$ and $t = 5$ min. Experimental k_L values (see Table 4) were determined for $C_{A0} = 100 \text{ mg L}^{-1}$.

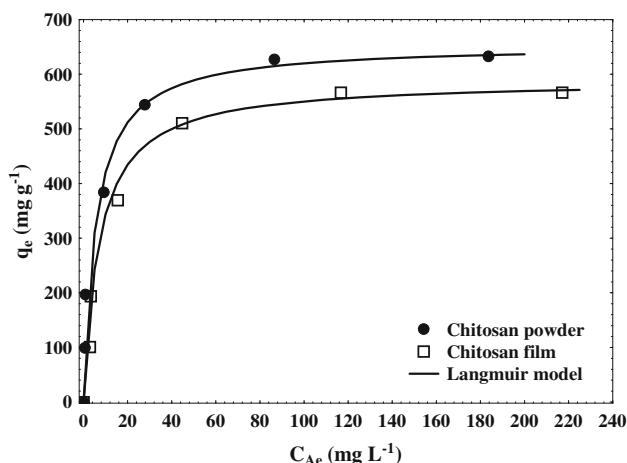


Fig. 3 Equilibrium curves for the RB5 adsorption on chitosan powder and chitosan films (298 K, pH = 4.0)

Table 3 Langmuir parameters for the RB5 adsorption on chitosan powder and chitosan films (298 K, pH = 4.0)

Parameter	Chitosan powder	Chitosan film
q_m (mg g ⁻¹)	654.3	589.5
K_L (L mg ⁻¹)	0.18	0.14
R^2	0.9936	0.9861
ARE (%)	1.31	1.57

The molecular diffusion coefficient of the RB5 in aqueous solution was estimated by the Wilke and Chang (1955) correlation (Eq. (15)):

$$D_{AB} = \frac{7.4 \times 10^{-8} (M_B)^{1/2} T}{\eta_B V_A^{0.6}} \tag{15}$$

where $\phi = 2.60$, $M_B = 18 \text{ g mol}^{-1}$, $\eta_B = 0.89 \text{ cp}$, and V_A value of RB5 was predicted by Le Bas method (Prausnitz and Tavares 2004). The molecular diffusion coefficient determined with Eq. (15) was $3.07 \times 10^{-6} \text{ cm}^2 \text{ s}^{-1}$.

The concentration decay curves of RB5 on chitosan materials were obtained at different stirring rates (50, 100, 200 and 400 rpm). Table 4 shows the operating conditions regarding the kinetic experiments. Figure 4 depicts as an example, the concentration decay curves of RB5 onto both adsorbents at 50, 100, 200 and 300 rpm.

In Fig. 4, it can be noticed that the adsorption equilibrium was not influenced by the stirring rate, besides in both systems the adsorption capacity was very similar, because at low equilibrium concentrations both adsorbate–adsorbent systems has identical behavior (see Fig. 3). Also, it is evident that the stirring rate has a major effect on the RB5–chitosan film system than on the RB5–chitosan powder, since the equilibrium time diminished from 1400 min to 400 min as the stirring rate increased from 50 to 300 rpm for chitosan films, whereas only decreased from 300 to 200 min for chitosan powder. This fact can be related with the S (Table 2) and k_L (Table 4) values. Chitosan film has lower S and k_L values than chitosan powder, leading to a slower adsorption rate at the initial stages. As consequence, the turbulence in mixing zone acts for more time, leading to a more pronounced effect.

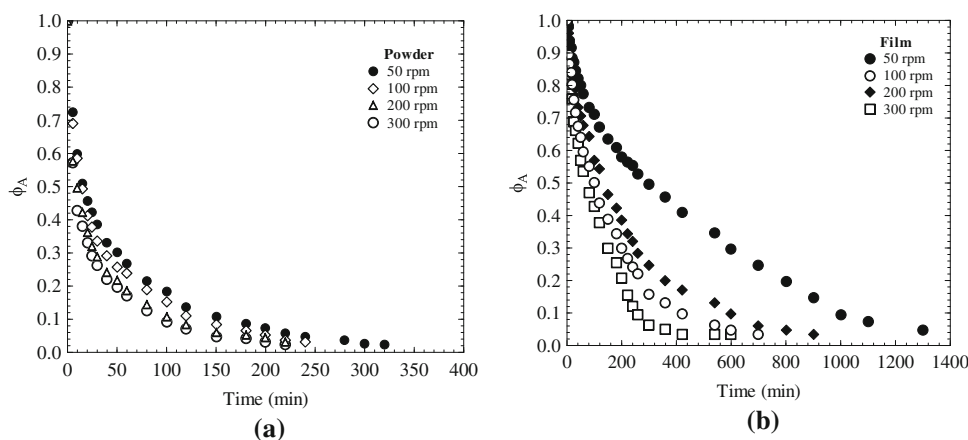
4.4 Application of EMTM and PVSDM models

In a stirred tank adsorber, the external mass transfer depends of the stirring rate, concentration gradient and particle size. In Fig. 4 is showed that the external mass transport plays a very important role on the adsorption rate

Table 4 Experimental conditions for the obtaining of concentration decay curves (pH 4, m = 0.1 g and V = 200 mL)

Exp.	C ₀ (mg L ⁻¹)	Stirring rate (rpm)	q _e (mg g ⁻¹)	k _L × 10 ³ (cm s ⁻¹)	D _s × 10 ¹¹ (cm ² s ⁻¹)
Chitosan powder					
1	100	50	195.14	3.23	2.85
2	100	100	194.36	3.65	3.75
3	100	200	196.86	4.97	4.84
4	100	300	193.24	5.00	5.78
Chitosan films					
5	100	50	193.05	0.55	4.15
6	100	100	193.56	1.20	7.80
7	100	200	193.27	3.30	7.84
8	100	300	194.73	3.50	12.12

Fig. 4 Concentration decay curves of RB5 onto chitosan **a** powder and **b** films at different stirring rates



of both adsorbate–adsorbent systems because it considerably affects the overall adsorption rate. Therefore the EMTM model was applied to predict the experimental data. The ordinary differential equations of the EMTM model were numerically solved using commercial software based in Runge–Kutta method. The experimental value of k_L needed for solving the EMTM model was estimated from Eq. (14). The experimental concentration decay curves of RB5 for run 4 and 8 and the concentration decay predicted with the EMTM model are depicted in Fig. 5a, b, respectively. In both figures, it is appreciated that the EMTM model predicts faster adsorption rates, since the concentration decay curves predicted with the EMTM model were below to the experimental concentration decay curves. As shown in Fig. 5a, b, the time to reach equilibrium prognosticated with the EMTM model was approximately 50 and 200 min, which are 3 and 2 folds faster than that obtained experimentally. Therefore, it is evident that the intraparticle diffusion played a very important role on the adsorption rate of RB5 on chitosan materials.

In the PVSDM model, the intraparticle diffusion is assumed to be due to both, pore volume diffusion and surface diffusion. The k_L values were estimated as argued

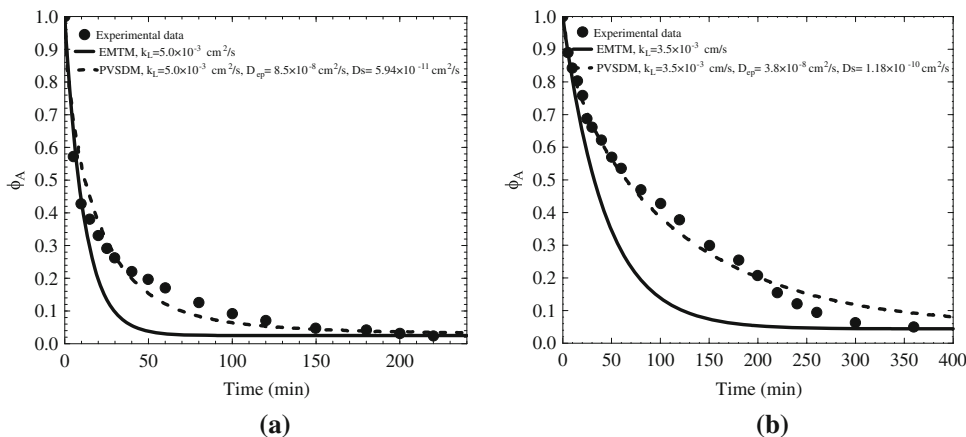
earlier. Thus, the surface diffusion coefficient, D_s and the effective diffusion coefficient, D_{ep} were the sole unknown mass transfer parameters and they can be calculated by fitting the numerical solution of the PVSDM model with the experimental concentration decay curve. In this case, the optimal values of D_s and D_{ep} were obtained through multi-parametric analysis using using Comsol Multiphysics, which is based in the finite element method. The number of the elements was one thousand and the solution was independent of the size mesh. Finally, the objective function that minimizes the Error is given by following equation.

$$\text{Error} = \int_{t=0}^{t=t} (C_{A,\text{exp}} - C_{A,\text{pred}})^2 dt \tag{16}$$

The concentration decay curves predicted with the PVSDM are plotted in Fig. 5a, b for Runs 4 and 8, respectively. As it can be observed in these figures, the PVSDM model satisfactorily fitted the experimental concentration decay data with values of D_{ep} = 8.5 × 10⁻⁸ and D_s = 5.94 × 10⁻¹¹ cm²/s for Run 4 and D_{ep} = 3.5 × 10⁻⁸ and D_s = 1.18 × 10⁻¹⁰ cm²/s for Run 8.

The contribution of each diffusion mechanism to the intraparticle mass transfer was estimated by computing the

Fig. 5 Concentration decay curves of RB5 on chitosan materials: **a** powder and **b** films. The *dash lines* represent the prediction of the EMTM model and the *solid lines* represent the fit of the PVSDM model



mass flux due to the pore volume diffusion, N_{AP} , and surface diffusion, N_{AS} , using the Eqs. (17) and (18):

$$N_{AP} = -D_{ep} \frac{\partial C_{Ar}}{\partial r} \tag{17}$$

$$N_{AS} = -D_s \rho_p \frac{\partial q}{\partial r} \tag{18}$$

Besides, the percentage contribution of surface diffusion to the intraparticle mass transfer can be calculated with the Eq. (19):

$$\frac{N_{AS}}{(N_{AS} + N_{AP})} 100\% = \frac{D_s \rho_p \frac{\partial q}{\partial r}}{D_s \rho_p \frac{\partial q}{\partial r} + D_{ep} \frac{\partial C_{Ar}}{\partial r}} 100\% \tag{19}$$

At various times, the percentage contribution of surface diffusion during adsorption of RB5 as a function of the particle radius for powder and film adsorbents is depicted in Fig. 6a, b, respectively. As shown in this figure, the contribution of surface diffusion was not dependent on the time and the radial position in the particle since the contribution of surface diffusion was always higher than 92%. Consequently, surface diffusion is much more important than pore volume diffusion in the adsorption rate RB5.

From these results, the SDM model was used to interpret the decay concentration curves of RB5 on both adsorbents.

Surface diffusion, i.e., the movement of the adsorbate through the solid surface, is influenced by the distribution of the solid and fluid phases, and the surface concentration gradients are the main driving force. In the SDM model, the intraparticle diffusion is exclusively due to surface diffusion and, therefore, pore volume diffusion can be ignored. This behavior can be considered, since the contribution of surface diffusion was always higher than 92% (see Fig. 6). The mass transfer parameters of the SDM model are k_L and D_s , and as described above, k_L was estimated with Eq. (14). The value of D_s was assessed by matching the numerical solution of the SDM model with the experimental concentration decay data. The best value of D_s was obtained by minimizing the objective function described by Eq. (16). Figure 7a, b shows as an example, the experimental data for the RB5 adsorption onto chitosan powder (Runs 1 and 2) and Fig. 7c, d does for chitosan films (Runs 5 and 6). Also in this figure, it is presented the prediction of the SDM model with the best value of D_s .

Figure 7 shows that the SDM model fitted very well the experimental data at different stirring rates. This

Fig. 6 Contribution of surface diffusion to the intraparticle diffusion at different radial positions. **a** Exp. 4 and **b** Exp. 8

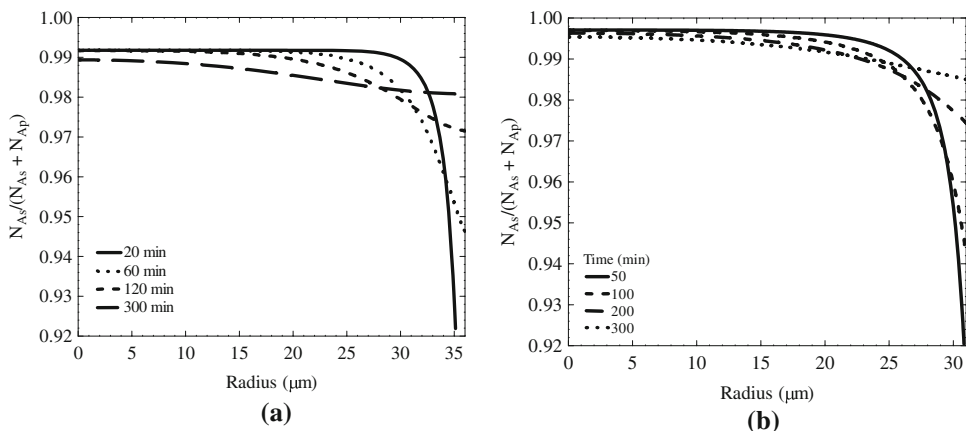


Fig. 7 Concentration decay curves of RB5 on chitosan materials: **a, b** powder and **c, d** films. The *dash lines* represent the prediction of the SDM model

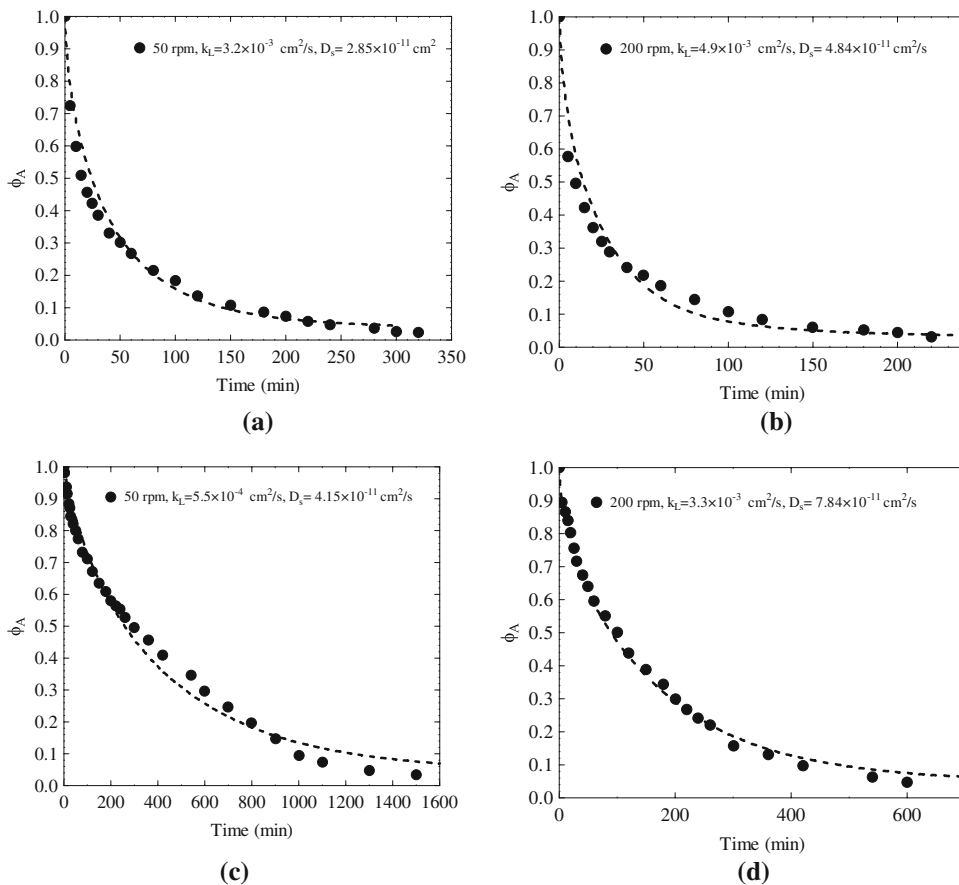
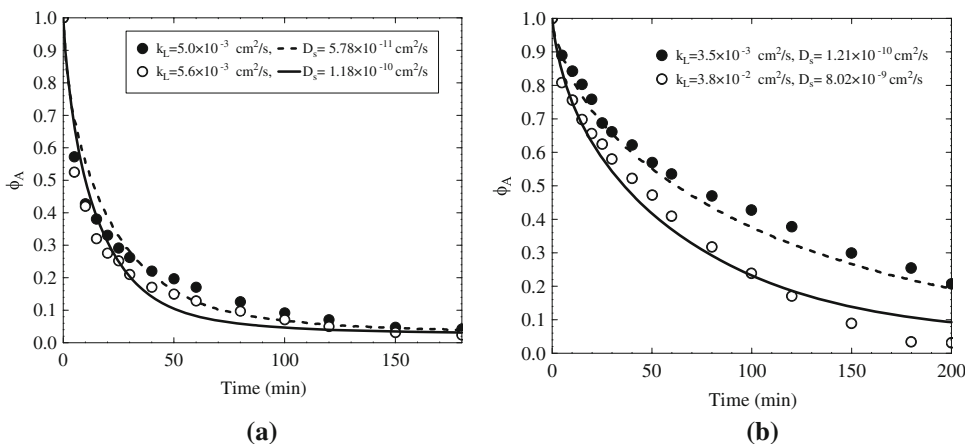


Fig. 8 Swelling effect on the concentration decay curves of RB5 on chitosan materials: **a** powder and **b** films. The *dash lines* represent the prediction of the SDM model for non-swelled material (*filled circle*) and the *solid lines* represent the fit of the SDM model for the swelled material (*open circle*)



corroborates that surface diffusion is the main mass transport mechanism involved in the intraparticle diffusion. Other two facts can be observed in Fig. 7: (i) the D_s values are slightly greater for the RB5–Films system than RB5–powder system. This can be attributed to the structure of powder and films (Fig. 2). Since CFS presented a more regular structure, the transference of dye molecules along the internal surface of chitosan films was facilitated. (ii) the D_s values increased with the stirring rate augment. This

fact has no physical mean, but, can be explained mathematically by Eq. (10) (with $D_{ep} = 0$). Higher k_L values were found at higher stirring rates. Consequently, to ensure the equality of Eq. (10), D_s should be also higher.

4.5 Swelling effect

Figure 8 shows the swelling effect on the adsorption decay curves of the systems RB5–films and RB5–powder. The

parameters k_L and D_s of the SDM model were estimated according to the Sect. 4.5. It was found in Fig. 8 that, for both, CPW and CFS, the D_s values increased when the adsorption was performed with the swelled material. This implies that RB5 adsorption due surface diffusion was faster for the swelled materials. During the swelling, the chitosan polymeric chains are expanded and the internal surface is smoothed due the repulsion between the protonated amino groups (Dotto et al. 2013). As consequence, the transference of RB5 molecules along the surface of the swelled materials was facilitated. Similar trend was found by Kyzas et al. (2012) studying the pre-swelling effect on adsorption dynamics of dyes by chitosan derivatives. Also, it can be seen that the swelling effect was most pronounced for chitosan films, providing an increase of about 65 times in the D_s value. This occurred since chitosan powder swelled 11.1 % while chitosan films swelled 86.2 % (Table 2).

5 Conclusion

The overall adsorption rate of RB5 dye onto chitosan powder (CPW) and chitosan films (CFS) was studied using external mass transfer model (EMTM), pore volume and surface diffusional model (PVSDM) and surface diffusional model (SDM). The geometry and swelling effects were considered. The EMTM predicted a faster rate in relation to the experimental values, indicating that intraparticle diffusion mechanism has important influence on the RB5 adsorption.

The application of PVSDM and SDM models revealed that the surface diffusion was much more important than pore volume diffusion in the adsorption rate of RB5 on both adsorbents, contributing with more than 92 % of the total intraparticle diffusion regardless to the position and time. The D_s values ranged from 2.85×10^{-11} to $8.02 \times 10^{-9} \text{ cm}^2 \text{ s}^{-1}$. The RB5 adsorption was faster when chitosan powder was used and, the swelling effect was most pronounced for chitosan films.

Acknowledgments The authors would like to thank CAPES (Coordination for the Improvement of Higher Education Personnel), CNPq (National Council for Scientific and Technological Development) and CEME-SUL (Federal University of Rio Grande Brazil). Dr. Raúl Ocampo Perez, acknowledges the support of the Consejo Nacional de Ciencia y Tecnología, CONACyT, Mexico, through CB-2013-01 221757.

References

- Ali, I., Asim, M., Khan, T.A.: Low-cost adsorbents for the removal of organic pollutants from wastewater. *J. Environ. Manag.* **113**, 170–183 (2012)
- Brunauer, S., Emmett, P.H., Teller, E.: Adsorption of gases in multimolecular layers. *J. Am. Chem. Soc.* **60**, 309–318 (1938)
- Chong, M.N., Tneu, Z.Y., Poh, P.E., Jin, B., Aryal, R.: Synthesis, characterisation and application of TiO₂-zeolite nanocomposites for the advanced treatment of industrial dye wastewater. *J. Taiwan Inst. Chem. Eng.* **50**, 288–296 (2015)
- Crini, G., Badot, P.M.: Application of chitosan, a natural aminopolysaccharide, for dye removal from aqueous solutions by adsorption processes using batch studies: a review of recent literature. *Prog. Polym. Sci.* **33**, 399–447 (2008)
- Demirbas, A.: Agricultural based activated carbons for the removal of dyes from aqueous solutions: a review. *J. Hazard. Mater.* **167**, 1–9 (2009)
- Dotto, G.L., Buriol, C., Pinto, L.A.A.: Diffusional mass transfer model for the adsorption of food dyes on chitosan films. *Chem. Eng. Res. Des.* **92**, 2324–2332 (2014)
- Dotto, G.L., Moura, J.M., Cadaval Jr., T.R.S., Pinto, L.A.A.: Application of chitosan films for the removal of food dyes from aqueous solutions by adsorption. *Chem. Eng. J.* **214**, 8–16 (2013)
- Dotto, G.L., Pinto, L.A.A.: Adsorption of food dyes acid blue 9 and food yellow 3 onto chitosan: stirring rate effect in kinetics and mechanism. *J. Hazard. Mater.* **187**, 164–170 (2011)
- Dotto, G.L., Sharma, S.K., Pinto, L.A.A.: Biosorption of organic dyes: research opportunities and challenges. In: Sharma, S.K. (ed.) *Green Chemistry for Dyes Removal from Waste Water: Research Trends and Applications*, pp. 295–329. Scrivener Publishing LLC, Beverly (2015)
- Dotto, G.L., Souza, V.C., Pinto, L.A.A.: Drying of chitosan in a spouted bed: the influences of temperature and equipment geometry in powder quality. *LWT Food Sci. Technol.* **44**, 1786–1792 (2011)
- Erdem, B., Erdem, M., Özcan, A.S.: Adsorption of Reactive Black 5 onto quaternized 2-dimethylaminoethyl methacrylate based polymer/clay nanocomposites. *Adsorption* (2016). doi:10.1007/s10450-016-9773-1
- Esquerdo, V.M., Cadaval Jr., T.R.S., Dotto, G.L., Pinto, L.A.A.: Chitosan scaffold as an alternative adsorbent for the removal of hazardous food dyes from aqueous solutions. *J. Colloid Interface Sci.* **424**, 7–15 (2014)
- Franco, D.S.P., Piccin, J.S., Lima, E.C., Dotto, G.L.: Interpretations about methylene blue adsorption by surface modified chitin using the statistical physics treatment. *Adsorption* **21**, 557–564 (2015)
- Furusawa, T., Smith, J.M.: Fluid-particle and intraparticle mass transport rates in slurries. *Ind. Eng. Chem. Fundam.* **12**, 197–203 (1973)
- Goldstein, J.I., Newbury, D.E., Echil, P., Joy, D.C., Romig Jr., A.D., Lyman, C.E., Fiori, C., Lifshin, E.: *Scanning Electron Microscopy and X-ray Microanalysis*. Plenum Press, New York (1992)
- Gupta, V.K., Suhas, I.: Application of low-cost adsorbents for dye removal: a review. *J. Environ. Manag.* **90**, 2313–2342 (2009)
- He, X., Du, M., Li, H., Zhou, T.: Removal of direct dyes from aqueous solution by oxidized starch cross-linked chitosan/silica hybrid membrane. *Int. J. Biol. Macromol.* **82**, 174–181 (2016)
- Koprivanac, N., Kusic, H.: *Hazardous Organic Pollutants in Colored Wastewaters*. New Science Publishers, New York (2008)
- Kyzas, G.Z., Kostoglou, M., Lazaridis, N.K.: Relating interactions of dye molecules with chitosan to adsorption kinetic data. *Langmuir* **26**, 9617–9626 (2010)
- Kyzas, G.Z., Lazaridis, N.K., Kostoglou, M.: Modelling the effect of pre-swelling on adsorption dynamics of dyes by chitosan derivatives. *Chem. Eng. Sci.* **81**, 220–230 (2012)
- Langmuir, I.: The adsorption of gases on plane surfaces of glass, mica and platinum. *J. Am. Chem. Soc.* **40**, 1361–1403 (1918)
- Mehrjouei, M., Müller, S., Möller, D.: A review on photocatalytic ozonation used for the treatment of water and wastewater. *Chem. Eng. J.* **263**, 209–219 (2015)

- Moura, J.M., Farias, B.S., Rodrigues, D.A.S., Moura, C.M., Dotto, G.L., Pinto, L.A.A.: Preparation of chitosan with different characteristics and its application for biofilms production. *J. Polym. Environ.* **23**, 470–477 (2015)
- Ocampo-Pérez, R., Leyva-Ramos, R., Alonso-Davila, P., Rivera-Utrilla, J., Sánchez-Polo, M.: Modeling adsorption rate of pyridine onto granular activated carbon. *Chem. Eng. J.* **165**, 133–141 (2010)
- Ocampo-Pérez, R., Leyva-Ramos, R., Mendoza-Barron, J., Guerrero-Coronado, R.M.: Adsorption rate of phenol from aqueous solution onto organobentonite: surface diffusion and kinetic models. *J. Colloid Interface Sci.* **364**, 195–204 (2011)
- Ocampo-Pérez, R., Leyva-Ramos, R., Rivera-Utrilla, J., Flores-Cano, J.V., Sánchez-Polo, M.: Modeling adsorption rate of tetracyclines on activated carbons from aqueous phase. *Chem. Eng. Res. Des.* **104**, 579–588 (2015)
- Ocampo-Pérez, R., Rivera-Utrilla, J., Gómez-Pacheco, C., Sánchez-Polo, M., López-Peñalver, J.J.: Kinetic study of tetracycline adsorption on sludge-derived adsorbents in aqueous phase. *Chem. Eng. J.* **213**, 88–96 (2012)
- Prausnitz, J.M., Tavares, F.W.: Thermodynamics of fluid-phase equilibria for standard chemical engineering operations. *AIChE J.* **50**, 739–761 (2004)
- Qiu, H., Pan, L.L., Zhang, Q.J., Zhang, W., Zhang, Q.: Critical review in adsorption kinetic models. *J. Zhejiang Univ. Sci.* **A10**, 716–724 (2009)
- Rêgo, T.V., Cadaval Jr, T.R.S., Dotto, G.L., Pinto, L.A.A.: Statistical optimization, interaction analysis and desorption studies for the azo dyes adsorption onto chitosan films. *J. Colloid Interface Sci.* **411**, 27–33 (2013)
- Ruthven, D.: Principles of Adsorption and Adsorption Processes. Wiley, New York (1984)
- Salleh, M.A.M., Mahmoud, D.K., Karim, W.A.W.A., Idris, A.: Cationic and anionic dye adsorption by agricultural solid wastes: a comprehensive review. *Desalination* **280**, 1–13 (2011)
- Saratale, R.G., Saratale, G.D., Chang, J.S., Govindwar, S.P.: Bacterial decolorization and degradation of azo dyes: a review. *J. Taiwan Inst. Chem. Eng.* **42**, 138–157 (2011)
- Silverstein, R.M., Webster, F.X., Kiemle, D.J.: Spectrometric Identification of Organic Compounds. Wiley, New York (2007)
- Srinivasan, A., Viraraghavan, T.: Decolorization of dye wastewaters by biosorbents: a review. *J. Environ. Manag.* **91**, 1915–1929 (2010)
- Su, C.X.H., Low, L.W., Teng, T.T., Wong, Y.S.: Combination and hybridisation of treatments in dye wastewater treatment: a review. *J. Environ. Chem. Eng.* (2016). doi:[10.1016/j.jece.2016.07.026](https://doi.org/10.1016/j.jece.2016.07.026)
- Suzuki, M.: Adsorption Engineering. Kodansha, Tokyo (1990)
- Thommes, M., Kaneko, K., Neimark, A.V., Olivier, J.P., Rodriguez-Reinoso, F., Rouquerol, J., Sing, K.S.W.: Physisorption of gases, with special reference to the evaluation of surface area and pore size distribution (IUPAC Technical Report). *Pure Appl. Chem.* **87**, 1051–1069 (2015)
- Vakili, M., Rafatullah, M., Salamatinia, M., Abdullah, A.Z., Ibrahim, M.H., Tan, K.B., Gholami, Z., Amouzgar, P.: Application of chitosan and its derivatives as adsorbents for dye removal from water and wastewater: a review. *Carbohydr. Polym.* **113**, 115–130 (2014)
- Verma, A.K., Dash, R.R., Bhunia, P.A.: A review on chemical coagulation/flocculation technologies for removal of colour from textile wastewaters. *J. Environ. Manag.* **93**, 154–168 (2012)
- Wilke, C.R., Chang, P.: Correlation of diffusion coefficients in dilute solutions. *AIChE J.* **1**, 264–268 (1955)
- Yagub, M.T., Sen, T.K., Afroze, S., Ang, H.M.: Dye and its removal from aqueous solution by adsorption: a review. *Adv. Colloid Interface Sci.* **209**, 172–184 (2014)